J Mater Sci: Mater Electron (2015) 26:3868–3873
DOI 10.1007/s10854-015-2913-7

Growth of ZnO nanorods and nanosheets by electrodeposition and their applications in dye-sensitized solar cells

Yu-Long Xie[1] · Jing Yuan[2] · Ping Song[1] · Shu-Qing Hu[1]

Received: 19 January 2015 / Accepted: 3 March 2015 / Published online: 11 March 2015

Abstract An electrochemical deposition process was used to synthesize zinc oxide (ZnO) nanorod and nanosheet structures on indium tin oxide substrate, which could tailored by a simple chemical route without templates and capping agents. The DSSCs based on three-dimensional (3D) ZnO nanosheet network structures showed more superior photoelectrochemical performance than that based on one-dimensional ZnO nanorods. The conversion efficiency of 1.59 % achieved by the DSSCs based on 3D ZnO nanosheet network structures. The improvement can be attributed to the enhanced dye loading, which is caused by the enlargement of internal surface area within the nanostructure photoelectrode. Furthermore, the polarity effects play a significant role on the photo-conversion efficiency.

1 Introduction

Dye-sensitized solar cells (DSSCs) have attracted great attention in the area of using clean solar energy [1–4]. DSSC is based on a mesoporous structure of a wide band semiconductor material [e.g., titanium oxide (TiO_2), zinc oxide (ZnO)] sensitized by a light harvesting material (conventionally metal–organic Ru-based dyes), permeated with a redox electrolyte, and sandwiched by a counter electrode. ZnO is a unique material that has prompted a vast amount of research. Various morphologies and sizes of ZnO materials have led to a wide range of promising applications. ZnO also is one of the most important semiconductor materials as the photoelectrodes of DSSCs and quantum dot sensitized solar cells (QDSSCs) due to its suitable energy-band structure and excellent physical properties [5]. Compared to TiO_2, ZnO is a rather unique functional semiconductor material with a wide band gap, higher electron mobility at room temperature (115–155 $cm^2\ V^{-1}\ s^{-1}$) is higher than that of anatase TiO_2 ($<10^{-5}\ cm^2\ V^{-1}\ s^{-1}$) [6], has been recognized as a kind of ideal material to replace TiO_2 [6–10]. In addition, the surface structures of ZnO can be easily controlled by growth methods, and have simple tailorability of nanostructure as compared to TiO_2 [7, 10, 11]. However, overall solar-to-electric energy conversion efficiency (η) of ZnO-based cells is still relatively low. In recent years, more researchers have been focused on improving the efficiency of ZnO-based cells using nanostructured ZnO materials, especially ZnO one-dimensional (1D) materials (nanowires, nanorods, nanowire/nanorod arrays and nanotubes et al.) which are believed to gain the enhancement of efficiency because of their rapid electron transfer, reduction of charge recombination degree, and collection of carriers through electrical transport pathway [7, 12–19]. However, the use of 1D ZnO nanomaterials limits the surface area and interface of electrode films, resulting in a low η.

Alternatively, another effective method to the enhance efficiency in DSSCs is to build a light scattering layer with enhanced photocapture efficiency and optical absorption in photoelectrode films [20–23]. Until now, a variety of ZnO nanostructures have been fabricated and applied in DSSCs and QDSSCs [19, 24, 25]. Although research related to the applications of ZnO is progressing rapidly, it has been an enormous change to produce uniform ZnO materials. There are many synthesis methods available to produce ZnO

✉ Yu-Long Xie
yulongxie2012@126.com

[1] College of Chemistry and Life Science, Qinghai University for Nationalities, Xining 810007, China

[2] College of Physics and Electronic Information Engineering, Qinghai University for Nationalities, Xining 810007, China

nanostructures, including thermal evaporation of ZnO powders [26], vapor-phase transport processes [27, 28], and solution synthesis [29–31]. Low-temperature process, high growth rate, ease of production on large-area substrate, and convenient operation are some of the advantages offered by electrodeposition, which are significant for further industrial applications. This work presents a simple electrochemical method for tuning the degree of extended growth of ZnO nanostructures along the c-axis, giving regular hexagonal sheet-like nanocrystals at one extreme and hexagonal rod at the other. The two-dimensional (2D) hexagonal sheet-like nanocrystals assembled to three-dimensional (3D) ZnO network nanostructures, was directly grown on ITO substrate at low temperature by electrochemical method, and its application on the photoelectrode of DSSCs was investigated by sensitizing the 3D ZnO nanosheets and 1D ZnO nanorods with N719. The QDSSCs based on the photoelectrode of 3D ZnO nanosheets network structures showed superior photoelectrochemical performance to that of 1D ZnO nanorods.

2 Experimental

In a typical electrodeposition process, a piece of Pt foil and a standard silver/silver chloride electrode (Ag/AgCl) were used as the counter and reference electrodes, respectively. Indium-tin oxide (ITO)-coated glass was used as a substrate and working electrode. ITO-coated glass was cleaned using acetone and rinsed with deionized water before use. All of the reagents are of analytical grade and used without further purification. Aqueous 0.1 M KCl solutions with various concentrations of $ZnCl_2$ were used as electrolytes. H_2O_2 was used as a source of oxygen. Electrodeposition was carried out using an electrochemical analytical instrument (Ivium Stat). The applied potential was operated at −1 V versus Ag/AgCl for 30 min and the solution temperature was maintained at 70 °C. Finally, all of the samples were annealed at 350 °C for 30 min in air.

For use in solar cells, the samples were dye-sensitized with Ru-based N719 dye (cis–bis (isothiocyanato) bis (2,2-bipyridyl 4,4-dicarboxylato) ruthenium(II) bis-tetrabutylammonium) by immersion in dye solution (mixture of acetonitrile and tert-butyl alcohol, volume ratio: 1:1) at 25 °C for 24 h. After dye-sensitization, the samples were rinsed with acetonitrile to remove non-chemisorbed dye and dried in a nitrogen stream. To measure dye-loading on the samples, the dye-sensitized ZnO layers were immersed in 4 mL of 10 mM KOH for 1 h, and afterwards the absortion spectra of the solutions were measured photometrically. To fabricate DSSCs, the ZnO samples were sensitized with Ru-based N719 dye and then sandwiched together with a Pt coated fluorine doped glass counter electrode using a polymer spacer (Surlyn). The electrolyte was a mixture of 0.1 M LiI, 0.03 M I_2, 0.6 M 1, 2-dimethyl-3-propylimidazolium iodide, and 0.5 M tert-butylpyridine (TBP) in acetonitrile.

The field-emission gun scanning electron microscope (FE-SEM, Hitachi S-4800) was used to evaluate the morphology of the samples. The crystalline orientations of TiO_2 were confirmed by X-ray diffraction (XRD-6000, Bruker). Photovoltaic measurements were made using an AM 1.5 illumination provided by a xenon lamp (150 W) with an optical filter (AM 1.5G) under a power of 100 mW cm^{-2} (calibrated by a standard silicon solar cell) and the Ivium Stat electrochemical analyzer was employed to measure the photocurrent and voltage (*J*–*V*) obtained from an illuminated area of 0.5 cm × 0.5 cm.

3 Results and discussion

The morphology of ZnO is a key factor in its properties. Many applications of ZnO nanostructures have been identified due to their morphological dependence. ZnO nanostructures can be synthesized by a variety of methods, such as chemical-vapor-deposition [32–34], thermal evaporation [35–37], hydrothermal synthesis [38–40], and electrodeposition process [41, 42]. Electrodeposition of ZnO nanostructures is generally based on the generation of OH^- ions at the surface of working electrode by electrochemical reduction of precursors such as O_2 [43], NO_3^- [44], and H_2O_2 [45] in Zn^{2+} aqueous solution. During the deposition process, OH^- ions are produced in terms of Eqs. (1), (2), or (3) after certain potential is applied. Then Zn^{2+} ions in the vicinity of working electrode react with OH^- ions, resulting in formation of zinc hydroxide ($Zn(OH)_2$) (Eq. 4). Finally, ZnO is produced by dehydration of $Zn(OH)_2$ (Eq. 5). The morphology of the as-synthesized ZnO nanodeposits strongly depends on the experimental conditions, particularly the Zn^{2+} concentration, which might change the reaction rate of the hydroxylation (Eq. 4) and dehydration (Eq. 5), thereby enabling modifying the growth behavior of ZnO nanodeposits [43, 46].

$$O_2 + 2H_2O + 4e^- \rightarrow 4OH^- \quad (1)$$

$$NO_3^- + H_2O + 2e^- \rightarrow NO_2^- + 2OH^- \quad (2)$$

$$H_2O_2 + 2e^- \rightarrow 2OH^- \quad (3)$$

$$Zn^{2+} + 2OH^- \rightarrow Zn(OH)_2 \quad (4)$$

$$Zn(OH)_2 \rightarrow ZnO + H_2O \quad (5)$$

The dehydration reaction plays a leading role in the electrolyte containing role in the electrolyte containing a low concentration of Zn^{2+} [43, 46]. Thus, $Zn(OH)_2$ can be

converted into ZnO as soon as it is produced, leading to formation of 1D ZnO nanostructures (e.g., nanorods, nanowires, or nanopillars) because of the anisotropic growth along the [0001] direction of the hexagonal wurtzite structure [43, 46–51]. However, the formation of ZnO produced by dehydration of $Zn(OH)_2$ could be delayed because of the relatively faster hydroxylation reaction in the case of high Zn^{2+} concentration. As a result, the growth along [0001] direction might be replaced by other preferred growth direction, such as $[01\bar{1}0]$ or $[10\bar{1}0]$ [39, 52], which can give rise to formation of 2D nanostructures (e.g., nanosheets or nanowalls) [42, 43, 46].

Figure 1a, b present the morphology of the ZnO nanostructures obtained at Zn^{2+} concentrations of 5 and 20 mM, respectively. It can be noticed that the morphology of ZnO nanostructures change from nanorods to nanosheets by increasing the Zn^{2+} concentration. The effect of Zn^{2+} concentration on the morphology can be attributed to the difference between the solubility of ZnO and other zinc-containing compounds, such as $Zn_5(OH)_8Cl_2H_2O$ [46]. At low Zn^{2+} concentration, ZnO has a lower solubility than $Zn_5(OH)_8Cl_2H_2O$ and is preferentially precipitated from the electrolyte at the electrode surface. Naturally, the *c*-axis of ZnO is associated with a higher growth rate than other directions and a rod-like morphology is therefore easily obtained. As the Zn^{2+} concentration is increased, the solubility of ZnO increases more rapidly than $Zn_5(OH)_8Cl_2H_2O$. In this case, Cl^- can partially substitute for OH^- and sheets-like $Zn_5(OH)_8Cl_2H_2O$ rather than ZnO nanorods is formed [53]. The formation of $Zn_5(OH)_8Cl_2$ can be attributed to the high concentration of Zn^{2+} in electrolyte, which gives rise to the large ionic products ($[Zn^{2+}][OH^-]_2$ or $[Zn^{2+}][OH^-]_x[Cl^-]_y$) in solution and hence the precipitation of $Zn(OH)_2$ (Eq. 4) or zinc hydroxylchloride compounds ($Zn(OH)_xCl_y$) (Eq. 6) in the as-synthesized nanodeposits, as demonstrated by Peulon and co-workers [43]. After annealing in the air, the pyrolysis of $Zn_5(OH)_8Cl_2H_2O$ will happen (Eq. 7).

$$Zn^{2+} + x(OH)^- + yCl^- \rightarrow Zn(OH)_xCl_y \quad (6)$$

$$Zn_5(OH)_8Cl_2H_2O \rightarrow 5ZnO + 4H_2O \uparrow + 2HCl \uparrow \quad (7)$$

Figure 1a is typical FE-SEM top-images of the as prepared films at low and high magnifications, respectively, showing a highly uniform and densely packed array of nanorods. The nanorods have flat hexagonal crystallographic planes, and their diameters are of 50–150 nm. While the sheet-like ZnO is formed with the increasing of Zn^{2+} concentration as shown in Fig. 1b. It is found that no nanorod structures are formed at the Zn^{2+} concentration of 20 mM, and 2D ZnO nanosheets are thus obtained. The 2D hexagonal sheet-like nanocrystals assembled to 3D ZnO network nanostructures.

Figure 2 shows the XRD patterns of ZnO nanostructures on ITO substrate. The positions of all diffraction peaks agreed closely with those of the wurtzite ZnO structure. Notably, the changing relative intensities of the (100) and (002) peaks in the XRD patterns of ZnO nanostructures

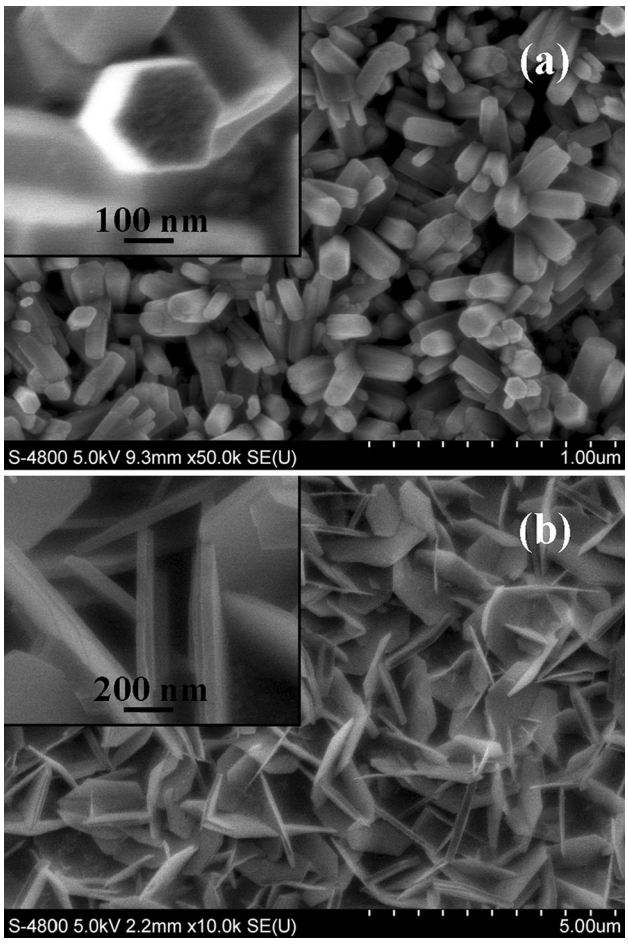

Fig. 1 **a** FE-SEM images of nanostructures electrodeposited on ITO substrates after thermal treatment with different $ZnCl_2$ concentration: **a** 5 mM; **b** 20 mM

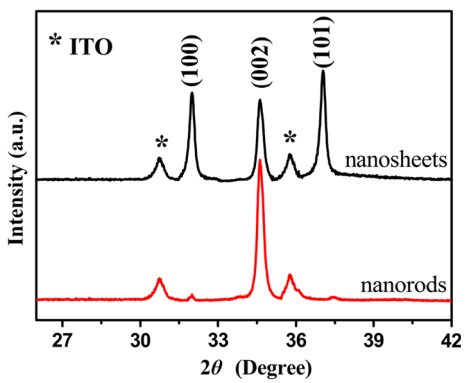

Fig. 2 XRD patterns of ZnO nanostructures with various morphologies

represent a change in shape [54]. A low (100)/(002) ratio reveals the formation of nanorods are oriented along the *c*-axis, and a large fraction of nonpolar facets. Conversely, a very large (100)/(002) ratio indicates shortening along the *c*-axis, as for a nanosheet structure, whose surface is dominated by polar facets. Accordingly, the XRD data herein clearly reveals that the significant difference between nanosheets and nanorods in the proportions of polar facets and nonpolar facets. The (001) and $(00\bar{1})$ polar planes of the wurtzite ZnO crystal are known to have a high surface energy, and the nonpolar planes parallel to the *c*-axis are the most stable and have a lower surface energy [53]. The polar facet of ZnO had a highest surface energy than any of the other faces. They have the inherent capacity to absorb the dye. At the same time, the polarity of wurtzite ZnO is a result of its noncentrosymmetric structure with its polar direction along the *c*-axis, this material exhibits strong spontaneous polarization ($P = -0.057$ cm^{-2}) [55]. The oppositely charged ions and the strong polarization field in the sheet structure may result in the efficient charge separation of photo-induced carrier.

The photovoltaic properties of the DSSCs constructed with the ZnO nanorod and nanosheet structures are presented in Fig. 3 and Table 1. The variation might be ascribed to the difference in the morphology of the ZnO nanostructures, which can therefore influence the internal surface area of the photoelectrodes. Thus the dye loading of the ZnO nanorod photoelectrode is restricted to the low level (2.86×10^{-8} mol cm^{-2}), leading to the low short-circuit current densities (Fig. 3 and Table 1) and hence the low power conversion efficiencies (1.15 %). Because of the relatively large internal surface area, the power conversion efficiency of the DSSCs increases to 1.59 %, which results in the high dye loading (3.54×10^{-8} mol cm^{-2}) and hence the high short-circuit current density (5.03 mA cm^{-2}). The high J_{sc} and η might be ascribed to the excellent properties of 3D ZnO nanosheet network structures. First, the large specific surface area of 3D ZnO nanosheet network structures increases the dye of N719 and light absorption intensity, and the high porosity facilitates the penetration of electrolyte in the photoelectrode. Second, the polar facet of ZnO nanosheet has a highest surface energy. Therefore, they have the inherent capacity to absorb the dye to increase the short-circuit current density. Finally, the efficient charge separation of photo-induced carriers is improved by the polarity of wurtzite ZnO which is a result of its noncentrosymmetric structure with its polar direction along the *c*-axis.

The photocatalytic activities of the ZnO nanorods and ZnO nanosheets were evaluated by studying the photocatalytic degradation of methylene blue (MB) in solution were tested under UV light. Methylene blue (MB), a typical dye contaminant in wastewater, is a blue cationic thiazine dye with maxima of absorbance at 660 (the most prominent), 614, and 292 nm. It has often been used as a model compound to test the photocatalytic degradation of organic materials [56]. All the samples with the size of 1 cm × 2.5 cm were soaked into two identical bottles containing MB (50 mg L^{-1}, 10 mL) and stored in a dark environment for 20 min to reach adsorption equilibrium of MB before exposure to UV light (254 nm, 8 W, 150 μW cm^{-2}) at a room temperature. Figure 4 compares the MB decomposition rate of all the samples over a period of time. After 140 min of photocatalytic reaction, 68 % of MB concentration was removed by sample ZnO nanorods,

Table 1 Photovoltaic performance parameters of DSSCs based on ZnO nanorod and nanosheet structures

DSSCs	J_{sc} (mA cm^{-2})	V_{oc} (V)	FF	η (%)	Amount of adsorbed dye ($\times 10^{-8}$ mol cm^{-2})
ZnO nanorods	3.33	0.61	0.56	1.15	2.86
ZnO nanosheets	5.03	0.63	0.52	1.59	3.54

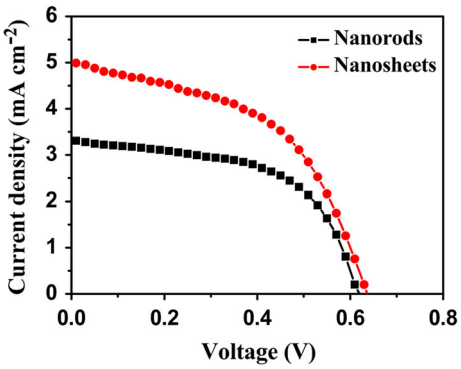

Fig. 3 *J–V* characteristics of DSSCs based on ZnO nanorod and nanosheet structures

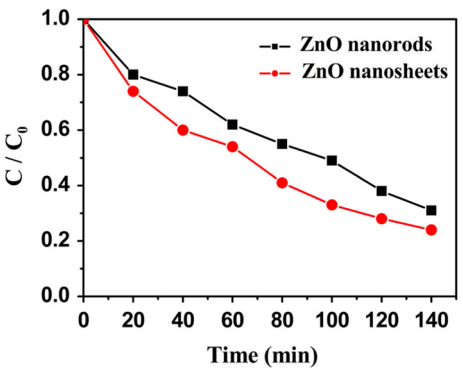

Fig. 4 Comparison of photocatalytic decomposition rates of MB of ZnO nanorods and ZnO nanosheets

and 77 % of MB concentration was removed by sample ZnO nanosheets, respectively. It is obviously that the ZnO nanosheets exhibited a much higher photocatalytic activity than the ZnO nanorods.

4 Conclusions

In summary, a simple chemical solution route for tailoring morphologies without template or capping agent was used successfully to shape ZnO into 1D nanorods and 2D nanosheets. The 2D hexagonal sheet-like nanocrystals assembled to 3D ZnO network nanostructures, which was directly grown on ITO substrate. The ZnO nanorods and nanosheets were used in the photoelectrode of DSSCs. The DSSCs based on 3D ZnO network nanostructures showed more superior photoelectrochemical performance than that based on 1D ZnO nanorods. The conversion efficiency of 1.59 % achieved by the DSSCs based on 3D ZnO nanosheet network structures. Based on this work, understanding the effect of morphology on photoelectrochemical activity can provide a blueprint for the design of materials in solar cell applications. The large specific surface area of 3D ZnO nanosheet network structures increases the dye loading. Moreover, the polarity effect can further play a significant role on the photo-conversion efficiency.

Acknowledgments The authors are grateful to the financial support from the Natural Science Foundation of Qinghai province (2013-Z-924Q and 2013-Z-901), and Chunhui Project of the Ministry of Education (Z2012109 and Z2012110).

References

1. B. O'Regan, M. Grätzel, A low-cost, high-efficiency solar cell based on dye-sensitized colloidal TiO_2 films. Nature **353**, 737–740 (1991)
2. K. Hara, K. Sayama, Y. Ohga, A. Shinpo, S. Suga, H. Arakawa, A coumarin-derivative dye sensitized nanocrystalline TiO_2 solar cell having a high solar-energy conversion efficiency up to 5.6 %. Chem. Commun. **6**, 569–570 (2001)
3. S. Ito, T. Kitamura, Y. Wada, S. Yanagida, Facile fabrication of mesoporous TiO_2 electrodes for dye solar cells: chemical modification and repetitive coating. Sol. Energy Mater. Sol. Cells **76**, 3–13 (2003)
4. K.M. Lee, V. Suryanarayanan, K.C. Ho, A study on the electron transport properties of TiO_2 electrodes in dye-sensitized solar cells. Sol. Energy Mater. Sol. Cells **91**, 1416–1420 (2007)
5. M.S. Akhtar, M.A. Khan, M.S. Jeon, O.-B. Yang, Controlled synthesis of various ZnO nanostructured materials by capping agents-assisted hydrothermal method for dye-sensitized solar cells. Electrochim. Acta **53**, 7869–7874 (2008)
6. E.M. Kaidashev, M. Lorenz, H. Wenckstern, A. Rahm, H.C. Semmelhack, K.H. Han, G. Benndorf, C. Bundesmann, H. Hochmuth, M. Grundmann, High electron mobility of epitaxial ZnO thin films on c-plane sapphire grown by multistep pulsed-laser deposition. Appl. Phys. Lett. **82**, 3901–3903 (2003)
7. M. Law, L.E. Greene, J.C. Johnson, R. Saykally, P. Yang, Nanowire dye-sensitized solar cells. Nat. Mater. **4**, 455–459 (2005)
8. R. Katoh, A. Furube, A.V. Barzykin, H. Arakawa, M. Tachiya, Kinetics and mechanism of electron injection and charge recombination in dye-sensitized nanocrystalline semiconductors. Coord. Chem. Rev. **248**, 1195–1213 (2004)
9. Q.F. Zhang, T.P. Chou, B. Russo, S.A. Jenekhe, G.Z. Cao, Polydisperse aggregates of ZnO nanocrystallites: a method for energy-conversion-efficiency enhancement in dye-sensitized solar cells. Adv. Funct. Mater. **18**, 1654–1660 (2008)
10. W. Lee, S.K. Min, V. Dhas, S.B. Ogale, S.-H. Han, Chemical bath deposition of CdS quantum dots on vertically aligned ZnO nanorods for quantum dots-sensitized solar cells. Electrochem. Commun. **11**, 103–106 (2009)
11. J.L. Gomez, O. Tigli, Zinc oxide nanostructures: from growth to application. J. Mater. Sci. **48**, 612–624 (2013)
12. Y.J. Lee, D.S. Ruby, D.W. Peters, B.B. McKenzie, J.W.P. Hsu, ZnO nanostructures as efficient antireflection layers in solar cells. Nano Letters **8**, 1501–1505 (2008)
13. T.W. Hamann, A.B.F. Martinson, J.W. Elam, M.J. Pellin, J.T. Hupp, Aerogel templated ZnO dye-sensitized solar cells. Adv. Mater. **20**, 1560–1564 (2008)
14. K. Wang, J.J. Chen, W.L. Zhou, Y. Zhang, Y.F. Yan, J. Pern, A. Mascarenhas, Direct growth of highly mismatched type II ZnO/ZnSe core/shell nanowire arrays on transparent conducting oxide substrates for solar cell applications. Adv. Mater. **20**, 3248–3253 (2008)
15. Y. Gao, M. Nagai, T.-C. Chang, J.-J. Shyue, Solution-derived ZnO nanowire array film as photoelectrode in dye-sensitized solar cells. Cryst. Growth Des. **7**, 2467–2471 (2007)
16. M. Guo, P. Diao, X. Wang, S.M.J. Cai, The effect of hydrothermal growth temperature on preparation and photoelectrochemical performance of ZnO nanorod array films. Solid State Chem. **178**, 3210–3215 (2005)
17. M. Guo, P. Diao, S.M. Cai, Photoelectrochemical properties of highly oriented ZnO nanotube array films on ITO substrates. Chin. Chem. Lett. **15**, 1113–1116 (2004)
18. C.Y. Jiang, X.W. Sun, G.Q. Lo, D.L. Kwong, J.X. Wang, Improved dye-sensitized solar cells with a ZnO-nanoflower photoanode. Appl. Phys. Lett. **90**, 263501 (2007)
19. H. Chen, W. Li, Q. Hou, H. Liu, L. Zhu, Growth of three-dimensional ZnO nanorods by electrochemical method for quantum dots-sensitized solar cells. Electrochim. Acta **56**, 8358–8364 (2011)
20. J. Ferber, J. Luther, Computer simulations of light scattering and absorption in dye-sensitized solar cells. Sol. Energy Mater. Sol. Cells **54**, 265–275 (1998)
21. A. Usami, Theoretical study of application of multiple scattering of light to a dye-sensitized nanocrystalline photoelectrichemical cell. Chem. Phys. Lett. **277**, 105–108 (1997)
22. G. Rothenberger, P. Comte, M. Grätzel, A contribution to the optical design of dye-sensitized nanocrystalline solar cells. Sol. Energy Mater. Sol. Cells **58**, 321–336 (1999)
23. Y.-Z. Zheng, X. Tao, L.-X. Wang, H. Xu, Q. Hou, W.-L. Zhou, J.-F. Chen, Novel ZnO-based film with double light-scattering layers as photoelectrodes for enhanced efficiency in dye-sensitized solar cells. Chem. Mater. **22**, 928–934 (2010)
24. B. Liu, H.C. Zeng, Fabrication of ZnO "dandelions" via a modified Kirkendall process. J. Am. Chem. Soc. **126**, 16744–16746 (2004)
25. M. Mo, J.C. Yu, L. Zhang, S.-K.A. Li, Self-assembly of ZnO nanorods and nanosheets into hollow microhemispheres and microspheres. Adv. Mater. **17**, 756–760 (2005)
26. Z.W. Pan, Z.R. Dai, Z.L. Wang, Nanobelts of semiconducting oxides. Science **291**, 1947–1949 (2001)

27. M.H. Huang, Y.Y. Wu, H.N. Feick, N. Tran, E. Weber, P.D. Yang, Catalytic growth of zinc oxide nanowires by vapor transport. Adv. Mater. **13**, 113–116 (2001)
28. M.H. Huang, S. Mao, H. Feick, H. Yan, Y. Wu, H. Kind, E. Weber, R. Russo, P. Yang, Room-temperature ultraviolet nanowire nanolasers. Science **292**, 1897–1899 (2001)
29. L. Vayssieres, K. Keis, S.-E. Lindquist, A. Hagfeldt, Purpose-built anisotropic metal oxide material: 3D highly oriented microrod array of ZnO. J. Phys. Chem. B **105**, 3350–3352 (2001)
30. L. Vayssieres, K. Keis, A. Hagfeldt, S.E. Lindquist, Three-dimensional array of highly oriented crystalline ZnO microtubes. Chem. Mater. **13**, 4395–4398 (2001)
31. L. Vayssieres, Growth of arrayed nanorods and nanowires of ZnO from aqueous solutions. Adv. Mater. **15**, 464–466 (2003)
32. J.B. Baxter, E.S. Aydil, Dye-sensitized solar cells based on semiconductor morphologies with ZnO nanowires. Sol. Energy Mater. Sol. Cells **90**, 607–622 (2006)
33. D.I. Suh, S.Y. Lee, T.H. Kim, J.M. Chun, E.K. Suh, O.B. Yang, S.K. Lee, The fabrication and characterization of dye-sensitized solar cells with a branched structure of ZnO nanowires. Chem. Phys. Lett. **442**, 348–353 (2007)
34. Y.B. Li, M.J. Zheng, L. Ma, M. Zhong, W.Z. Shen, Fabrication of hierarchical ZnO architectures and their superhydrophobic surfaces with strong adhesive force. Inorg. Chem. **47**, 3140–3143 (2008)
35. J.Y. Lao, J.G. Wen, Z.F. Ren, Hierarchical ZnO nanostructures. Nano Lett. **2**, 1287–1291 (2002)
36. P.X. Gao, Z.L. Wang, Self-assembled nanowire–nanoribbon junction arrays of ZnO. J. Phys. Chem. B **106**, 12653–12658 (2002)
37. J.Y. Lao, J.Y. Huang, D.Z. Wang, Z.F. Ren, ZnO nanobridges and nanonails. Nano Lett. **3**, 235–238 (2003)
38. C.Y. Jiang, X.W. Sun, G.Q. Lo, D.L. Kwong, J.X. Wang, Improved dye-sensitized solar cells with a ZnO-nanoflower photoanode. Appl. Phys. Lett. **90**, 263501 (2007)
39. H.M. Cheng, W.H. Chiu, C.H. Lee, S.Y. Tsai, W.F. Hsieh, Formation of branched ZnO nanowires from solvothermal method and dye-sensitized solar cells applications. J. Phys. Chem. C **112**, 16359–16364 (2008)
40. T.R. Zhang, W.J. Dong, M. Keeter-Brewer, S. Konar, R.N. Njabon, Z.R. Tian, Site-specific nucleation and growth kinetics in hierarchical nanosyntheses of branched ZnO crystallites. J. Am. Chem. Soc. **128**, 10960–10968 (2006)
41. L.F. Xu, Q.W. Chen, D.S. Xu, Hierarchical ZnO nanostructures obtained by electrodeposition. J. Phys. Chem. C **111**, 11560–11565 (2007)
42. J. Qiu, M. Guo, X. Wang, Electrodeposition of hierarchical ZnO nanorod–nanosheet structures and their applications in dye-sensitized solar cells. ACS Appl. Mater. Interfaces **3**, 2358–2367 (2011)
43. S. Peulon, D. Lincot, Mechanistic study of cathodic electrodeposition of zinc oxide and zinc hydroxychloride films from oxygenated aqueous zinc chloride solutions. J. Electrochem. Soc. **145**, 864–874 (1998)
44. M. Izaki, T. Omi, Transparent zinc oxide films prepared by electrochemical reaction. Appl. Phys. Lett. **68**, 2439–2440 (1996)
45. T. Pauporte, D. Lincot, Hydrogen peroxide oxygen precursor for zinc oxide electrodeposition I. Deposition in perchlorate medium. J. Electrochem. Soc. **148**, C310–C314 (2001)
46. D. Pradhan, K.T. Leung, Controlled growth of two-dimensional and one-dimensional ZnO nanostructures on indium tin oxide coated glass by direct electrodeposition. Langmuir **24**, 9707–9716 (2008)
47. R. Tena-Zaera, J. Elias, G. Wang, C. Levy-Clement, Role of chloride ions on electrochemical deposition of ZnO nanowire arrays from O_2 reduction. J. Phys. Chem. C **111**, 16706–16711 (2007)
48. J. Elias, R. Tena-Zaera, C. Levy-Clement, Effect of the chemical nature of the anions on the electrodeposition of ZnO nanowire arrays. J. Phys. Chem. C **112**, 5736–5741 (2008)
49. D. Pradhan, M. Kumar, Y. Ando, K.T. Leung, Fabrication of ZnO nanospikes and nanopillars on ITO glass by templateless seed-layer-free electrodeposition and their field-emission properties. ACS Appl. Mater. Interfaces **1**, 789–796 (2009)
50. T. Pauporte, G. Bataille, L. Joulaud, F.J. Vermersch, Well-aligned ZnO nanowire arrays prepared by seed-layer-free electrodeposition and their Cassie–Wenzel transition after hydrophobization. J. Phys. Chem. C **114**, 194–202 (2010)
51. H. El Belghiti, T. Pauporte, D. Lincot, Mechanistic study of ZnO nanorod array electrodeposition. Phys. Status Solidi A **205**, 2360–2364 (2008)
52. D. Pradhan, K.T. Leung, Vertical growth of two-dimensional zinc oxide nanostructures on ITO-coated glass: effects of deposition temperature and deposition time. J. Phys. Chem. C **112**, 1357–1364 (2008)
53. Y.-K. Hsu, Y.-G. Lin, Y.-C. Chen, Polarity-dependent photoelectrochemical activity in ZnO nanostructures for solar water splitting. Electrochem. Commun. **13**, 1383–1386 (2011)
54. A. Mclaren, T. Valdes-Solis, G. Li, S.C. Tsang, Shape and size effects of ZnO nanocrystals on photocatalytic activity. J. Am. Chem. Soc. **131**, 12540–12541 (2009)
55. G. Bruno, M.M. Giangregorio, G. Malandrino, P. Capezzuto, I.L. Fragala, M. Losurdo, Is there a ZnO face stable to atomic hydrogen? Adv. Mater. **21**, 1700–1706 (2009)
56. H. Fu, T. Xu, S. Zhu, Y. Zhu, Photocorrosion inhibition and enhancement of photocatalytic activity for ZnO via hybridization with C. Environ. Sci. Technol. **42**, 8064–8069 (2008)